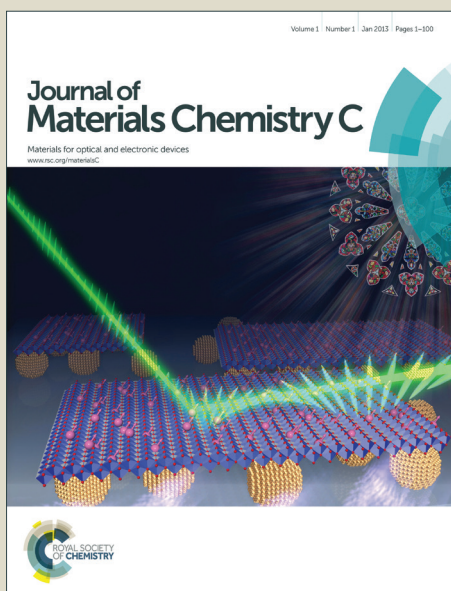


Journal of Materials Chemistry C

Accepted Manuscript



This is an *Accepted Manuscript*, which has been through the Royal Society of Chemistry peer review process and has been accepted for publication.

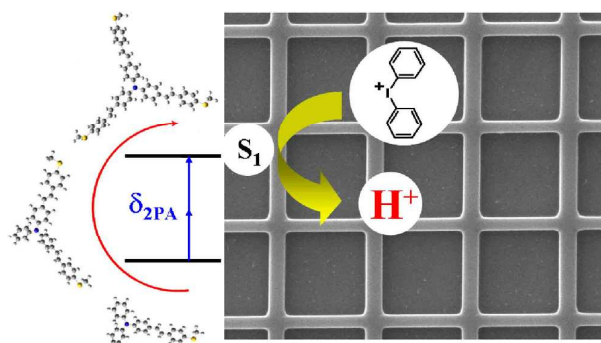
Accepted Manuscripts are published online shortly after acceptance, before technical editing, formatting and proof reading. Using this free service, authors can make their results available to the community, in citable form, before we publish the edited article. We will replace this *Accepted Manuscript* with the edited and formatted *Advance Article* as soon as it is available.

You can find more information about *Accepted Manuscripts* in the [Information for Authors](#).

Please note that technical editing may introduce minor changes to the text and/or graphics, which may alter content. The journal's standard [Terms & Conditions](#) and the [Ethical guidelines](#) still apply. In no event shall the Royal Society of Chemistry be held responsible for any errors or omissions in this *Accepted Manuscript* or any consequences arising from the use of any information it contains.

Table of Contents

Branching effects lead to a cooperative enhancement of the two-photon absorption (2PA) in the NIR (800 nm) and visible range (532 nm).



Two-Photon Lithography in Visible and NIR Ranges Using Multibranch-based Sensitizers For Efficient Acid Generation

Cite this: DOI: 10.1039/x0xx00000x

Received 00th January 2012,

Accepted 00th January 2012

DOI: 10.1039/x0xx00000x

www.rsc.org/

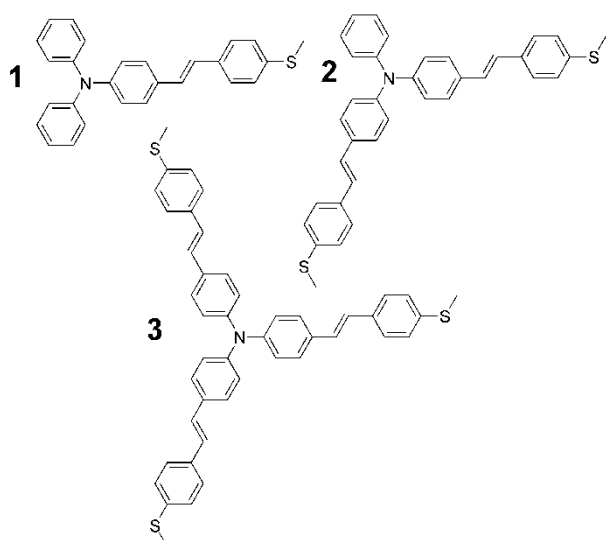
Ming Jin^{*,a}, Jianchao Xie^a, Jean-Pierre Malval^{*,b}, Arnaud Spangenberg^b, Olivier Soppera^b, Davy-Louis Versace^c, Tiffanie Leclerc^b, Haiyan Pan^a, Decheng Wan^a, Hongting Pu^a, Patrice Baldeck^d, Olivier Poizat^e and Stephan Knopf^b

We investigated methodically the one- and two-photon absorption properties of a series of multibranch triphenylamine-based chromophores incorporating 4-(methylthio)styryl fragments as external substituents. Some relevant structures/properties relationships relative to these highly fluorescent compounds have been derived based on emission anisotropy measurements, quantum chemical calculations and the use of the exciton coupling theory. Even though branching effects lead to a cooperative enhancement of the two-photon absorption (2PA), all compounds exhibit relatively low-to-moderate 2PA cross-sections ($\delta \leq 100$ GM) in the NIR region. However, the 'so-called' one-photon resonance enhancement effect leads to a remarkable increase of δ by more than one order of magnitude in the visible range. This strong 2PA ability has been associated with an efficient photosensitization of iodonium salt to elaborate a new bicomponent photoacid generator which is readily two-photon activable at 532 nm. In the visible range, the strong enhancement of the efficiency of the two-photon induced polymerization is clearly demonstrated as compared with that observed in the NIR region.

1. INTRODUCTION

Multiphoton excitation constitutes an emergent technology with a rapid development due to the promising applications in a very wide range of domains including three-dimensional fluorescence imaging¹, photodynamic therapy², high density optical data storage³ or two-photon fabrications⁴⁻¹¹. By tightly focusing an excitation beam and taking advantage of the very low probability for the two-photon absorption (2PA) event, a spatial confinement of all primary and subsequent photo-induced processes are promoted. This fundamental concept has strongly stimulated the engineering research for the design and the elaboration of various molecular architectures which both associate a large 2PA ability and more specific properties oriented toward the final applications^{1, 12}. Photoacid generators (PAGs) are compounds that can release acid upon irradiation¹³. They constitute an important class of cationic photoinitiators which have a strategic position in the polymer industries^{14, 15}. Commercially available PAGs are mainly photoactivated through direct excitation at wavelengths ranging from VUV to close UV¹⁶⁻²². Moreover they exhibit very low 2PA cross-sections because of their limited π -conjugation²³. It has been

extensively demonstrated that the photolysis of PAGs can be readily sensitized using visible absorbing dyes^{13, 24} such as fluoflavin²⁵ or acridinedione²⁶ ($\lambda_{\text{exc}} \sim 420$ nm), Benzoflavin²⁷ ($\lambda_{\text{exc}} \sim 460$ nm), Acridine Orange²⁷ ($\lambda_{\text{exc}} \sim 540$ nm) or phenoxazin²⁸ ($\lambda_{\text{exc}} \sim 600$ nm). The acid generation generally proceeds through an intermolecular photoinduced electron transfer (PeT) from the excited sensitizer to the PAG. Due to the inherent diffusion limitation of the global kinetics associated to this bimolecular process, an alternative strategy has been proposed and consists in a direct incorporation of the acid generator functionality into the structure of the sensitizer. Interestingly, both direct and indirect strategies are valuable for the two-photon induced acid generation and have been fruitfully applied for multiphoton lithography^{7, 29-43}. For instance, Perry *et al.*²⁹⁻³² have proposed a direct excitation strategy with the design of a sulfonium-based D- π -D derivative which both exhibits high quantum yield for acid generation ($\Phi_{\text{H}^+} \sim 0.5$) and large 2PA cross sections ($\delta \sim 690$ GM). This two-photon activable PAG shows an impressive two-photon *action* cross-section ($\delta \cdot \Phi_{\text{H}^+}$) of about 345 GM. More recently our working group has extended this pioneer approach with the



Scheme 1. Molecular structures of sensitizers 1-3.

elaboration of several D- π -A sulfonium-based PAGs^{7, 36} in which a strong enhancement of Φ_{H^+} was demonstrated through a para-to-meta positioning effect of the sulfonium substituent. From a conceptual point of view, this direct excitation strategy should present superior performances as the bimolecular approach. But from a practical point of view, this latter method seems more competitive due to its facile and economic processing steps which do not required complicated and time-consuming synthesis. For instance, Wu *et al.*⁴⁴ have recently associated the well known N-(trifluoromethanesulfonyloxy)-1,8-naphthalimide photoacid generator¹⁸⁻²⁰ with various two-photon activable dibenzilidene ketones. In this example, the low quantum yield for acid generation ($\Phi_{\text{H}^+} \sim 0.053$) was strongly counterbalanced by the very large 2PA cross-section ($\delta \sim 1000$ GM) of the sensitizers leading to a two-photon *action* cross-section of 53 GM.

The present contribution reports a distinctive approach for the two-photon sensitizing of diphenyliodonium salt based on a multibranch sensitizer series (**Scheme 1**). Indeed, the multibranch strategy constitutes a relevant tool to modulate both linear and nonlinear absorption properties without drastic impacts on the energy position of the electronic transitions⁴⁵⁻⁴⁸. Therefore, these compounds maintain an excellent transparency in a large part of the visible region which becomes suitable for two-photon lithography. In this spectral range, we show that our bicomponent systems appear as highly-reactive two-photon acid generators with a large two-photon *action* cross-section ($\delta \cdot \Phi_{\text{H}^+}$) with maximum value up to 117 GM.

2. Experimental Section

2.1 Materials and general methods

All synthesis reagents were purchased from Energy Company (Shanghai, China). Diphenyliodonium hexafluorophosphate (PAG), 2-isopropylthioxanthone (**ITX**), the cycloaliphatic diepoxide monomer, namely 3,4-Epoxy cyclohexylmethyl-3,4-

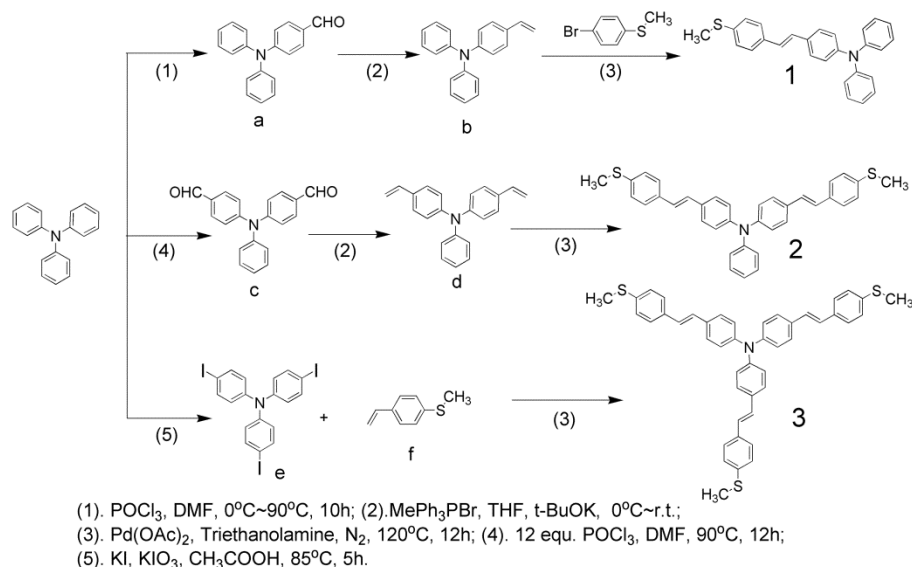
epoxycyclohexanecarboxylate (EPOX), were supplied by Aldrich. The SU-8 photoresist (SU-8 2075) was purchased without photoinitiator from Microchem company. All the solvents employed were Aldrich, Fluka or Merck spectroscopic grade. Proton and carbon nuclear magnetic resonance spectra (¹H, ¹³C NMR) were recorded on a Bruker Avance 500 (400 MHz) spectrometer. Chemical shifts were reported in parts per million (ppm) downfield from the Me₄Si resonance which was used as the internal standard when recording NMR spectra. Element analysis was performed by Elementar Vario El III (Germany). Mass spectra were recorded on a Micromass GCTTM.

2.2 Synthesis and characterization of the compounds

The general synthetic route for the synthesis of the compounds **1**, **2** and **3** is depicted in **Scheme 2**. All compounds were synthesized by Heck coupling reactions in considerable yields (50-60 %). The precursors 4-(N, N'-diphenylamino)benzaldehyde (**a**), 4-(N, N'-diphenylamino)styrene (**b**), 4,4'-diformyl-triphenylamine (**c**), triiodo-triphenylamine (**e**), 4-methylthiostyrene (**f**), and compound **1**, namely (*E*)-4-methylthio-4'-N, N'-diphenylamino-stilbene, were readily obtained according to the literature procedures^{36, 49-51}. All new compounds were identified and characterized by ¹H NMR, ¹³C NMR spectroscopy, mass spectrometry and elemental analysis.

SYNTHESIS OF N, N'-BIS(4-VINYLPHENYL)BENZENAMINE (D). Potassium *tert*-butoxide (5.2 g, 46.4 mmol) is added to a solution of triphenylmethylphosphonium bromide (23.2 g, 57.2 mmol) in 50 mL of dry THF at 0 °C. The solution is then stirred during 15 min at this temperature before addition of compound (**c**) (7.2 g, 24.0 mmol). After 3 h of reaction at room temperature, the solution is poured into 400 mL of water. The solid was collected by filtration. The crude product was recrystallized in ethyl alcohol to give white solid (90.0 % in yield). ¹H NMR (400 MHz, CDCl₃, ppm): δ 7.29 (d, *J* = 8.6 Hz, 4H, PhH), 7.24 (d, *J* = 8.4 Hz, 2H, PhH), 7.09 (d, *J* = 7.6 Hz, 2H, PhH), 7.03 (m, 5H, PhH), 6.69-6.62 (m, 2H, CH = CH), 5.64 (d, *J* = 17.6 Hz, 2H, CH = CH), 5.16 (d, *J* = 10.9 Hz, 2H, CH = CH). MS (MALDI-TOF): *m/z* 298.15 [M + H⁺] (Calcd for C₂₂H₁₉N: 297.15). Anal. Calcd (%) for C₂₂H₁₉N: C, 88.85; H, 6.44; N, 4.71, Found: C, 88.89; H, 6.47; N, 4.64.

SYNTHESIS OF N, N'-BIS(4-(*E*)-4-(METHYLTHIO)STYRYL)PHENYL)BENZENAMINE (2). 4-bromothioanisole (2.22 g, 0.11 mol), compound (**d**) (1.49 g, 0.05 mol) and palladium (II) acetate (10 mg, 0.045 mmol) are added to triethanolamine (8 mL). The solution is stirred during 10 hours at 120°C under N₂-atmosphere. The mixture is then cooled to room temperature, poured into cold water (100 mL) and extracted with dichloromethane (50 mL \times 3). The collected organic layer is then washed three times with brine and dried over anhydrous magnesium sulfate. The solid product is filtered using a short pad of silica gel. The residual dichloromethane is removed at reduced pressure leading to a crude product which is redissolved in a 1v/1v mixture solution of chloroform and ethanol at 80 °C. A pale yellowish powder is finally obtained



Scheme 2. Reaction route for the synthesis of triphenylamine-based sensitizers **1**, **2** and **3**.

after a slow cooling down to 0 °C. The product is filtered off, dried in vacuum and weight (1.62 g, 60.0 % in yield). ¹H NMR (400 MHz, CDCl₃, ppm): δ 7.38 (dd, *J* = 11.6, 8.5 Hz, 8H, PhH), 7.29 – 7.19 (m, 6H, PhH), 7.12 (d, *J* = 7.7 Hz, 2H, PhH), 7.06 (d, *J* = 8.6 Hz, 5H, PhH), 7.01 (d, *J* = 16.3 Hz, 2H, CH = CH), 6.94 (d, *J* = 16.3 Hz, 2H, CH = CH), 2.48 (s, 6H, CH₃). ¹³C NMR (100 MHz, CDCl₃, ppm): δ 147.35, 147.05, 137.56, 134.70, 131.98, 129.48, 127.62, 127.45, 126.91, 126.83, 124.85, 124.06, 123.46, 16.01; MS (MALDI-TOF): *m/z* 542.19 [*M* + H⁺] (Calcd for C₃₆H₃₁NS₂: 541.19). Anal. Calcd (%) for C₃₆H₃₁NS₂: C, 79.81; H, 5.77; N, 2.59; Found: C, 79.89; H, 5.47; N, 2.64.

SYNTHESIS OF TRIS(4-((E)-4-(METHYLTHIO)STYRYL)PHENYL)AMINE (3). 4-methylthiostyrene (2.5 g, 0.016 mol), tris(4-iodophenyl)amine (**e**) (3.11 g, 0.005 mol) and palladium (II) acetate (20.0 mg, 0.090 mmol) are added to a mixed solution of triethanolamine (15 mL) and *N,N*-Dimethyl acetamide (15 mL). The stirred mixture is heated to 120 °C during 20 hours under N₂-atmosphere. The mixture is then cooled to room temperature, poured into cold water (100 mL) and extracted with dichloromethane (50 mL × 3). The purification process is same as (**2**) and a bright yellowish powder is finally obtained (1.75 g, 51.0 % in yield). ¹H NMR (400 MHz, CDCl₃): δ 7.39 (t, *J* = 6.9 Hz, 9H, PhH), 7.30 (d, *J* = 7.8 Hz, 2H, PhH), 7.22 (d, *J* = 7.6 Hz, 7H, PhH), 7.16 – 7.06 (m, 6H, PhH), 7.02 (d, *J* = 17.2 Hz, 4H, CH = CH), 6.95 (d, *J* = 16.3 Hz, 2H, CH = CH), 2.48 (s, 9H, CH₃). ¹³C NMR (100 MHz, CDCl₃, ppm): δ 146.81, 137.64, 134.65, 132.28, 129.21, 128.90, 127.51, 126.86, 126.33, 124.37, 16.00; MS (MALDI-TOF): *m/z* 690.23 [*M* + H⁺] (Calcd for C₄₅H₃₉NS₃: 689.22). Anal. Calcd (%) for C₄₅H₃₉NS₃: C, 78.33; H, 5.70; N, 2.03; Found: C, 78.39; H, 5.67; N, 2.04.

2.3 Instrumentation and methods

The absorption measurements were carried out with a Perkin Elmer Lambda 2 or a Shimadzu 2550 double beam UV-vis spectrophotometers. Steady-state fluorescence spectra were collected from a FluoroMax-4 spectrofluorometer. Emission spectra are spectrally corrected, and fluorescence quantum yields include the correction due to solvent refractive index and were determined relative to quinine bisulfate in 0.05 molar sulfuric acid ($\Phi = 0.52$)⁵².

For the steady-state anisotropy measurements, two Glan-Thompson polarizers are placed in the excitation and emission beams. The anisotropy *r* is determined as follows:

$$r = \frac{I_{VV} - gI_{VH}}{I_{VV} + 2 \cdot g \cdot I_{VH}} \quad \text{with } g = \frac{I_{HV}}{I_{HH}}$$

Where *I* is the fluorescence intensity. The subscripts denote the orientation (horizontal *H* or vertical *V*) of the excitation and emission polarizers, respectively. *g* is an instrumental correction factor. The proper calibration of the set-up was checked using a recent standard method with rhodamine 101 in glycerol⁵³.

The fluorescence lifetimes were measured using a Nano LED emitting at 372 nm as an excitation source with a nano LED controller module, Fluorohub from IBH, operating at 1MHz. The detection was based on an R928P type photomultiplier from Hamamatsu with high sensitivity photon-counting mode. The decays were fitted with the iterative reconvolution method on the basis of the Marquardt/Levenberg algorithm⁵⁴. Such a reconvolution technique allows an overall-time resolution down to 0.15 ns. The quality of the exponential fits was checked using the reduced χ^2 (≤ 1.2).

The two-photon absorption (2PA) measurements were performed with femtosecond mode-locked laser pulse using a

Ti: Sapphire laser (Coherent, Chameleon Ultra II: pulse duration: ~140 fs; repetition rate: 80 MHz; wavelength range: 680-1040 nm). A second-harmonic generator module (Harmonics from Coherent) positioned after the oscillator enables to extend the excitation wavelength to the 340-520 nm range. A relative two-photon excited fluorescence (2PEF) method⁵⁵ was employed to measure the two-photon absorption cross-sections, δ . The measurements of 2PA cross-sections were performed relative to reference molecules (r) such as fluorescein^{55, 56} in water at pH = 11 ($\Phi_{\text{fluo}} = 0.90$) and 9,9-Didecyl-N²,N⁷-bis(4-methoxyphenyl)-N²,N⁷-diphenyl-9H-fluoren-2,7-diamine^{57, 58} (DAF) in N,N-dimethylformamide ($\Phi_{\text{fluo}} = 0.60$). The value of δ for a sample (s) is given by:

$$\delta_s = \frac{S_s \Phi_r \eta_r c_r}{S_r \Phi_s \eta_s c_s} \cdot \delta_r$$

Where S is the detected two-photon excited fluorescence integral area, c the concentration of the compounds, and Φ is the fluorescence quantum yield of the compounds. η is the collection efficiency of the experimental set-up and accounts for the wavelength dependence of the detectors and optics as well as the difference in refractive indices between the solvents in which the reference and sample compounds are dissolved. The measurements were conducted in a regime where the fluorescence signal showed a quadratic dependence on the intensity of the excitation beam, as expected for two-photon induced emission. For the calibration of the two-photon absorption spectra, the two-photon excited fluorescence signal of each compound was recorded at the same excitation wavelength as that used for standards (i.e. $\lambda_{\text{exc}} = 782$ nm for fluorescein ($\delta = 38$ GM) and $\lambda_{\text{exc}} = 520$ nm for DAF ($\delta = 80$ GM)). The concentration of the solutions was about 10^{-4} M for all compounds. In order to reduce the inner filter effects, the optical length for the collection of the fluorescence signal has been minimized in the cuvette by positioning the excitation focal point very close to the detection window. A typical 2PEF spectrum using such a nearly 'front-face' configuration is shown in Fig. S1 (†ESI) and compared to the 1PEF spectrum. One clearly observes that the 2PEF band matches that recorded upon one photon excitation. The laser intensity was in the range of $0.2 - 2 \times 10^9$ W/cm². The experimental error on the reported cross section is 15 %.

Quantum yields for acid generation were measured under irradiation at 365 nm using a 100 W Mercury-Xenon Lamp (Hamamatsu, L2422-02) equipped with a band pass filter. All irradiated PAGs dissolved in acetonitrile were previously N₂-degassed. The progress of the photoreaction was monitored via UV-vis absorption spectra. The absorbance at the excitation wavelength ($A_{365 \text{ nm}}$) was greater than 2.5 to assume a total absorption of the incident photons. The dose rates were kept sufficiently small so that the changes of $A_{365 \text{ nm}}$ were lower than 10 %. The Rhodamine B (RhB) was used as a sensor of photoacid generation as typically illustrated in Fig. S2 (†ESI).

The acid generation in acetonitrile was also evaluated from a calibration curve of RhB which was gradually protonated by addition of p-toluenesulfonic acid³². Then, photoacid quantum yields were calculated according the equation:

$$\Phi_{H^+} = \frac{V_{\text{sol}}}{l_{\text{cell}} \cdot S_{\text{irr}}} \frac{N_A}{\epsilon_{555 \text{ nm}}^{\text{RhB}}} \left| \frac{dA_{555 \text{ nm}}}{dt} \right| I_0 (1 - 10^{-A_{365 \text{ nm}}})$$

Where V_{sol} , l_{cell} and S_{irr} correspond to the volume of the irradiated solution, the optical path and the irradiated surface respectively. N_A is the Avogadro number. $A_{555 \text{ nm}}$ and $\epsilon_{555 \text{ nm}}$ correspond to the absorbance and the molar extinction coefficient of RhB. Finally, the incident light intensity at 365 nm (I_0) were measured by ferrioxalate actinometry⁵⁹.

The cyclic voltammetry experiments⁶⁰⁻⁶² (using a computer-controlled Radiometer Voltlab 6 potentiostat with a three-electrode single compartment cell; the working electrode was a platinum disk; a saturated calomel electrode (SCE) used as a reference was placed in a separate compartment with a salt bridge containing the supporting electrolyte) were performed at 300 K, in N₂-degassed dichloromethane with a constant concentration (0.1 M) of n-Bu₄NBF₄. Ferrocene (Fc) was used as an internal reference (considering $E_{\text{Fc}/\text{Fc}^+} = 0.53$ V in CH₂Cl₂ vs. aqueous SCE⁶³).

The photopolymerization was monitored *in situ* by Fourier transform real-time infrared spectroscopy (FT-RTIR) with a Thermo-Nicolet 6700 instrument IR-spectrometer. A drop of the photocurable formulation is deposited on a KBr pellet then spread out with a calibrated bar. The aerated film which exhibits an average thickness of 40 μm is irradiated at 365 nm using a Xe-Hg lamp (Hamamatsu, L8252, 150 W) equipped with a band pass filter. The conversion rates are derived from the changes in the infrared absorption bands of the monomer. The regions of interest correspond to the decrease in the epoxide absorption bands in the 800-900 cm⁻¹ region which corresponds to the C-H bond stretching vibration of epoxide and to the increase of the peaks at 1050-1150 cm⁻¹ assigned to the absorption of the (C-O-C) groups in the poly(ether) which is produced upon photopolymerization^{64, 65}.

The highly viscous SU-8 photoresist (SU8-2075 from Microchem, $\eta_{20^\circ\text{C}} = 22$ Pa.s) used for 2D-stereolithography was dissolved in cyclohexanone (50 wt. %) and mixed with the bicomponent photoacid generator: **3**/(Ph₂I⁺,PF₆⁻): 0.15 wt. % (2.5 mM)/1.5 wt.% (40 mM). The resin is then coated at 3000 rpm. Soft-baking of the SU-8 and evaporation of the solvent are conducted at 95 °C during 10 min. After the two-photon exposure, a post-baking at 95 °C during 5 min. leads to the appearance of μ -structures. The unlinked regions were finally developed using cyclohexanone.

The 3D lithographic microfabrication was carried out using a Zeiss Axio Observer D1 inverted microscope^{66, 67}. The two-photon excitation was performed at 800 nm and at 532 nm using respectively a mode-locked Ti: Sapphire oscillator (Coherent, Chameleon Ultra II: pulse duration: ~140 fs;

repetition rate: 80 MHz) and a frequency doubled Nd-YAG microlaser Nanolaser from JDS Uniphase ($\lambda_{\text{exc}} = 532$ nm, pulse duration 0.61 ns, maximum pulse energy 6 μJ , repetition 11.8 kHz). The incident beam was focused through a 0.65 NA objective (40 \times) which leads to radial spot sizes of 400 nm at $\lambda_{\text{exc}} = 532$ nm and 600 nm at $\lambda_{\text{exc}} = 800$ nm ($1/e^2$ Gaussian). A SU-8 photoresist with bicomponent photoacid generators were spin-coated on a cover slip which is mounted on a 3D piezoelectric stage allowing the translation relative to the laser focal point that can be adjusted by the two-photon induced fluorescence. The intensity of the entering laser is controlled with the use of an acousto-optic modulator. The displacement of the sample and all exposure parameters (i.e. excitation power and irradiation time which depends on the scan rates of the laser focal point) are computer-controlled. In order to compare the feature widths of the two-photon lithography at different irradiated wavelength (532 nm and 800 nm), the same scan rates are used. This entire lithography set-up was purchased from Teemphotonics Company.

The theoretical absorption spectra have been computed based on Density Functional Theory (DFT) and Time-Dependent DFT (TD-DFT). The overall computation strategy was defined as follows: After initial AM1 optimization calculations (vacuum), subsequent optimization of geometrical structures of the derivatives were carried out using the PBE0/6-31G(d) level of calculation. (Note that PBE0 is a good functional for the description of photofunctional molecules⁶⁸). Finally, the TD-DFT vertical transitions have been computed using the same level of calculations. All calculations have been performed using GAUSSIAN 09 package⁶⁹.

3. RESULTS AND DISCUSSION

3.1 Photophysical features of the compounds.

SYMMETRY AND ELECTRONIC PROPERTIES OF THE GROUND STATES. The absorption spectra of the compounds in dichloromethane are depicted in Fig. 1. Table 1 gathers all corresponding spectroscopic and electrochemical data. For all compounds, the low energy side of the spectra is dominated by

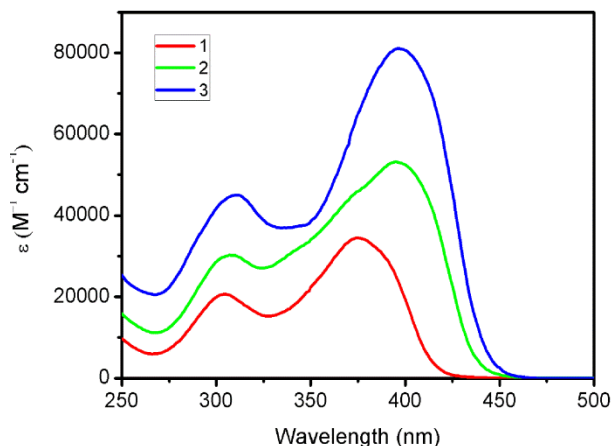


Fig. 1. Absorption spectra of sensitizers 1-3 in dichloromethane.

Table 1. Spectroscopic and electrochemical data of sensitizers in dichloromethane. Calculated dipole moment changes ($\Delta\mu_{\text{ge}}$) between ground and emitting states.

	$\lambda_{\text{abs}}/\text{nm}$ (eV)	$\epsilon_{\text{max}}/\text{M}^{-1}\text{cm}^{-1}$	$E_{\text{ox}}^a/\text{V vs.SCE}$	$\Delta\mu_{\text{ge}}/\text{D}$
1	374 (3.32)	34500	0.94	14.1
2	394 (3.14)	53200	0.91	13.3
3	395 (3.14)	81000	0.90	14.4

^a Irreversible oxidation peaks.

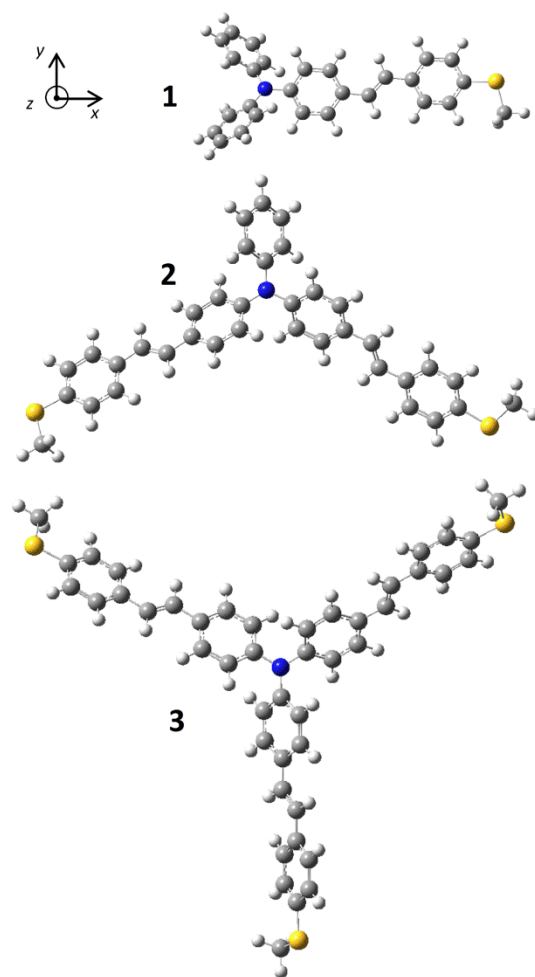


Fig. 2. Optimized geometry of sensitizers 1-3 (PBE0/6-31G(d) level).

a single and structureless band which increases in intensity and undergoes a bathochromic shift on going from 1 to 3. Note that the maximum molar extinction coefficient (ϵ_{MAX}) gradually increases from $34500\text{ M}^{-1}\text{ cm}^{-1}$ to $81000\text{ M}^{-1}\text{ cm}^{-1}$ whereas the band redshift clearly levels off when considering the multibranching compounds. Therefore, the quadrupolar and three-branched compounds constitute remarkable UV-Visible absorbing dyes which offer an excellent linear transparency within a large part of the visible-NIR region. Two slight shoulders are also observed at the blue edge of longest

Table 2. TD-DFT and experimental electronic transitions of sensitizers **1-3**.

	1				2				3			
	Exp. E_{00}/eV	Theoretical E_{th}/eV	f	Pol. ^a	Exp. E_{00}/eV	Theoretical E_{th}/eV	f	Pol. ^a	Exp. E_{00}/eV	Theoretical E_{th}/eV	f	Pol. ^a
$S_0 \rightarrow S_1$	3.14	3.17	1.32	x	3.00	2.95	1.70	x	2.95	2.89	1.38	x
$S_0 \rightarrow S_2$		3.90	0.03	x,z		3.31	0.40	y		2.90	1.45	y
$S_0 \rightarrow S_3$		4.00	0.27	x		3.71	0.42	y		3.45	- ^b	x,y
$S_0 \rightarrow S_4$						3.81	0.05	y,z		3.67	0.69	x
$S_0 \rightarrow S_5$						3.91	0.63	x		3.67	0.67	y

^a xyz axis are displayed in Fig. 2; ^b $f < 0.001$

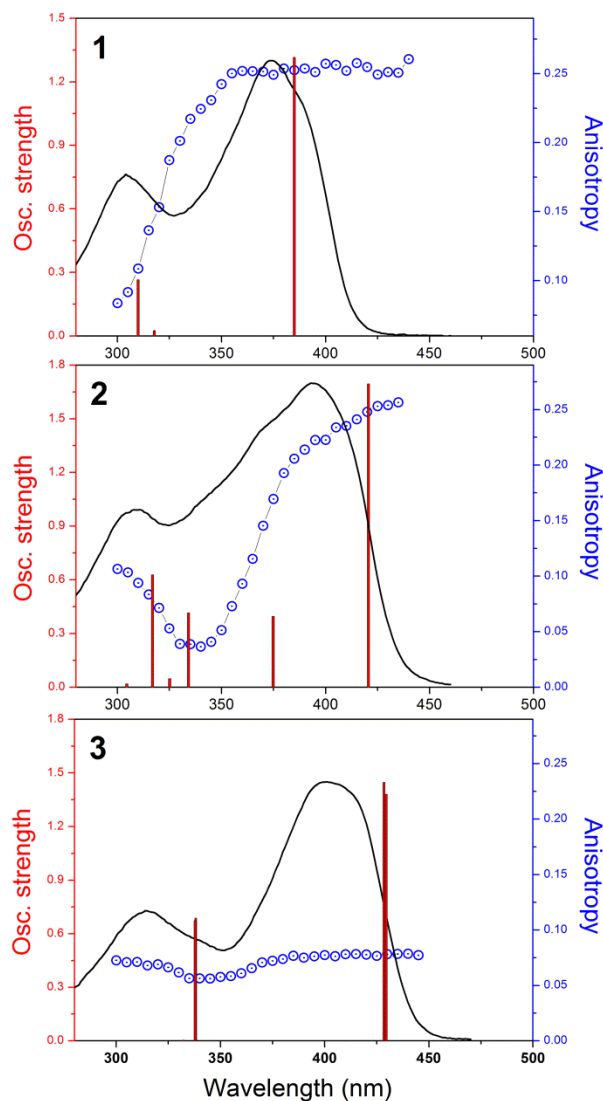
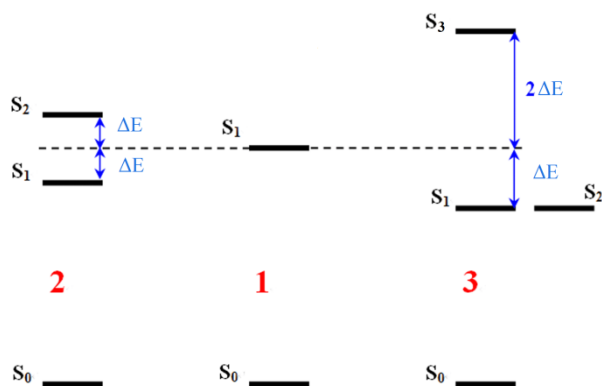


Fig. 3. Absorption (full lines) and excitation anisotropy spectra (circles) of **1-3** in triacetin. Positions of vertical energy transitions (vertical bars) along with corresponding electronic oscillator strengths calculated from the TD-DFT method.

wavelength absorption band for compound **2**. This suggests the presence of multiple $S_0 \rightarrow S_n$ electronic transitions as will be highlighted hereafter. Finally all these compounds exhibit a second distinctive band near 300 nm which is usually observed

for N-phenylated stilbene systems⁷⁰ and should be ascribed to electronic transitions centered on the triphenylamine moiety⁷¹. The fully optimized structures of compounds calculated at DFT level are presented in Fig. 2. All three dyes show quite similar structures since the 4-(methylthio)styryl branches adopt a quasi-planar conformation and the triphenyl moiety globally presents a D_3 -like symmetry with twist angles around the bond connecting the central nitrogen atom to the phenylene rings of about 35° to 39° . Such equivalencies of the ground states geometry are also in line with the redox properties of the compounds which exhibit quite equivalent oxidation potential whose average value is about 0.92 V vs. SCE (see Table 1). Such a potential is relatively low as compared to that of the triphenylamine (1.20 V vs. SCE). This clearly indicates an increase of the charge density which should be mainly localized on the amine core. To determine the position of the $S_0 \rightarrow S_n$ electronic transitions within the absorption spectra of the compounds, steady-state excitation anisotropy measurements have been performed in viscous medium (i.e. triacetin, $\eta_{20^\circ\text{C}} = 25$ mPa.s). Fig. 3 shows the corresponding anisotropy spectra along with the calculated absorption spectra using TD-DFT method based on the fully optimized geometries of **1-3**. And Table 2 shows the calculated energies of the electronic transitions with their corresponding oscillator strengths and the main orientation of their transition dipole moments. We also add in Table 2 the experimental values of the 0-0 transition energies (E_{00}). This parameter was measured from the intercept of the normalized absorption and fluorescence spectra recorded at in apolar solvent (i.e. Hexane). As shown in Table 2, the calculated $S_0 \rightarrow S_1$ transition energy agrees quite well with the experimental E_{00} . For all compounds, the longest wavelength electronic transition is strongly allowed ($f > 1$) and corresponds to a pure HOMO-LUMO transition which implies an electronic delocalization all along the compound structure (π - π^* type) with a very slight charge transfer from the amino group to the styryl moieties (see frontier molecular orbitals in Fig. S3, †ESI). As depicted in Fig. 3, the theoretical absorption spectra nicely reproduce the general trends observed for the experimental evolution of the excitation anisotropy spectra. For the dipolar compound **1**, the anisotropy remains constant in the 350-450 nm range which confirms the presence of a well isolated electronic transition. The anisotropy of **1** then undergoes a strong decrease below 340 nm which is also in line with the presence of other $S_0 \rightarrow S_n$



Scheme 3. Schematic representation of the effects of the interbranch coupling on the electronic levels for the two- and three-branched sensitizers.

transitions (with $n \geq 3$). For the quadrupolar compound **2**, the evolution of the spectrum is more complex since the anisotropy undergoes a sequential decrease on going from 435 to 380 nm. These changes can be ascribed to the presence of the $S_0 \rightarrow S_1$ and $S_0 \rightarrow S_2$ transitions located in the same spectral range. It should be emphasized that these latter transitions exhibit distinctive polarizations (see Table 2). Below 375 nm, the anisotropy of **2** first drops drastically and reaches a plateau in the 330–345 nm range then increases on going to the high energy part of the spectrum. These multiple changes in the anisotropy spectrum globally agree with the position of the main transitions $S_0 \rightarrow S_3$ and $S_0 \rightarrow S_5$. Finally, the compound **3** shows a similar anisotropy evolution with regard to that of **2**. However, the anisotropy of **3** is globally weak with an average value of ca. 0.07 ± 0.01 in the low energy side of the spectrum. In this region, the calculations indicate the presence of two strongly allowed transitions (i.e. $S_0 \rightarrow S_1$ and $S_0 \rightarrow S_2$) which are very close in energy (< 0.05 eV) and have different polarizations. The same observations can be done with the presence of the S_4 and S_5 transitions in the 335–350 nm range and leads to a very slight change in anisotropy.

The multi-branched compound **2** and **3** can be seen as the association of two and three dipolar monomer **1** respectively. According to the Frenkel exciton model^{72, 73}, the interbranch electrostatic interactions can lead to the splitting of the initially degenerate single excited levels associated to each molecular synthon⁴⁸. Depending on the nature and the strength of the interbranch coupling, these interactions can give rise to multiple electronic $\pi-\pi^*$ transitions. As illustrated in Scheme 3, for a homo-dimeric compound (e.g. quadrupole **2**), a symmetrical splitting of the two-fold degenerated S_1 levels occurs. The strength of the interbranch coupling (ΔE) corresponds to half the S_1 – S_2 energy gap. In the same manner, if we consider a homo-trimeric compound with D_3 symmetry (e.g. octupole **3**), the electronic level diagram exhibits a two-fold degenerated S_1 state and a third non-degenerated S_2 state which is shifted by $+3(\Delta E)$ from the S_1 levels. For both multibranched dipoles, the Frenkel model provides a reasonable picture of the experimental and theoretical results. In the case of compound **1** (i.e. 3.17 eV). Therefore, the interbranch of the compound **2**,

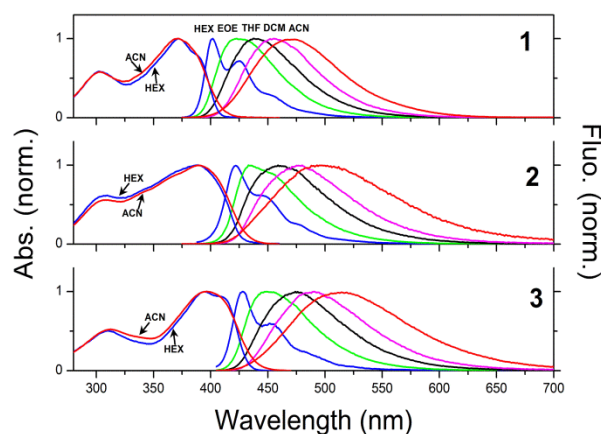


Fig. 4. Normalized absorption and fluorescence spectra of **1-3** in solvents of different polarity.

the midpoint energy between S_1 (2.95 eV) and S_2 (3.31 eV) levels matches quite well the S_1 energy of coupling (ΔE) can be roughly estimated to ca. 0.18 eV. For the compound **3**, the first two states are quasi-degenerate ($E_2 - E_1 = 0.01$ eV), whereas the S_3 level is positioned at 0.56 eV above the first two excited states. Note that the $S_0 \rightarrow S_3$ transition is weakly allowed with $f = 0.0007$. The coupling constant for **3** can also be estimated to ca. 0.19 eV. Interestingly, this coupling constant is comparable to that obtained for **2** (0.18 eV) which is in good accordance with the structural equivalencies observed for their respective ground state geometries (see Fig. 2), especially the similar distances and relative orientations of the interacting dipoles.

FLUORESCENCE AND EXCITED STATES PROPERTIES. Fig. 4 shows the normalized absorption and fluorescence spectra of the compounds in various solvents of increasing polarity and Table 3 gathers some related spectroscopic data. Contrary to the absorption spectra, the fluorescence bands undergo a pronounced bathochromic shift with increasing solvent polarity. This solvent induced effect provides a clear evidence for the charge transfer (CT) character of the fluorescence singlet states. For the compounds **2** and **3**, such a significant electronic relaxation also confirms a symmetry breaking in the charge delocalization between the Franck-Condon excited state whose excitation is fully delocalized within the entire multibranched structures and the emitting states whose excitation is only localized on a single branch of the compound. Such an effect has been theoretically predicted and observed for the relaxed S_1 state of multibranched compounds with quadrupolar V-shaped geometries^{46, 47} or octupolar trigonal symmetries^{45, 74}. The dipole moment change ($\Delta\mu_{ge}$) between ground and excited states can be estimated using the Lippert-Mataga equation^{75, 76}(eq. 1):

$$\Delta\nu_{ST} = \frac{2\Delta\mu_{eg}^2}{hca_0^3} \left[\frac{\epsilon - 1}{2\epsilon + 1} - \frac{n^2 - 1}{2n^2 + 1} \right] + Const. \quad (1)$$

Table 3. Maxima of UV absorption and fluorescence in various solvents. Fluorescence quantum yields, fluorescence decay times, radiative and nonradiative rate constants.

1	$\lambda_{abs} / \text{nm}$	$\lambda_{fluo} / \text{nm}$	Φ_{fluo}	τ / ns	$k_r^b / 10^9 \text{ s}^{-1}$	$k_{nr}^c / 10^9 \text{ s}^{-1}$
HEX ^a	372	401	0.71	1.02	0.70	0.28
EOE	371	425	0.89			
THF	374	437	0.93	2.00	0.47	0.04
DCM	377	454	0.87	2.02	0.43	0.06
ACN	371	470	0.65	2.43	0.27	0.14
2	$\lambda_{abs} / \text{nm}$	$\lambda_{fluo} / \text{nm}$	Φ_{fluo}	τ / ns	$k_r^b / 10^9 \text{ s}^{-1}$	$k_{nr}^c / 10^9 \text{ s}^{-1}$
HEX ^a	388	421	0.41	1.02 (0.80) 1.66 (0.20)	0.36	0.51
EOE	391	454	0.81			
THF	394	461	0.81	2.28	0.36	0.08
DCM	391	477	0.79	2.38	0.33	0.09
ACN	390	497	0.33	1.26 (0.27) 2.40 (0.73)	0.16	0.32
3	$\lambda_{abs} / \text{nm}$	$\lambda_{fluo} / \text{nm}$	Φ_{fluo}	τ / ns	$k_r^b / 10^9 \text{ s}^{-1}$	$k_{nr}^c / 10^9 \text{ s}^{-1}$
HEX ^a	395	428	0.66	1.25 (0.65) 1.38 (0.35)	0.51	0.26
EOE	396	452	0.90			
THF	401	476	0.77	2.33	0.33	0.10
DCM	403	488	0.77	2.42	0.32	0.10
ACN	396	514	0.44	0.61 (0.13) 2.48 (0.87)	0.20	0.25

^a HEX: Hexane, EOE: Diethylether, THF: Tetrahydrofuran, DCM: Dichloromethane, ACN: Acetonitrile. ^b $k_r = \Phi_{fluo} / \langle \tau \rangle$. ^c $k_{nr} = (1 - \Phi_{fluo}) / \langle \tau \rangle$

Within this dielectric continuum model, ϵ is the relative permittivity and n the refractive index of the solvent, h is the Planck constant and c is the speed of light. The Onsager radius a_0 defined as the solvent shell around the molecule was estimated to a value of ca. 5.5 Å. This value corresponds to 40 % of the longest axis of the compound **1** as suggested by Lippert for non-spherical molecules⁷⁵. The solvatochromic plots of Stokes shifts are shown in Fig. S4 (†ESI) and values for $\Delta\mu_{eg}$ are summarized in Table 1. For all compounds, $\Delta\mu_{ge}$ are of the same order of magnitude with values in the 13-15 D range. It confirms a photoinduced charge transfer (CT) enhancement presumably from the amino donor group to a styryl branch. It is interesting to note that the estimated values for $\Delta\mu_{ge}$ are equivalent to that obtained for the 4-(N, N'-diphenylamino)stilbene⁷¹ (~ 14 D) which indicates a relatively weak inductive effect of the methylthio substituent as confirmed by its Hammett constant ($\sigma_{para}^{Hammett} = 0.00$). As shown in Table 3, all compounds show very high quantum yields with minimum values close to 0.8 in moderately polar and polar solvents. The highly emissive character of the relaxed excited state is also illustrated when comparing the radiative (k_r) and non-radiative (k_{nr}) rate constants. In dichloromethane, for instance, the radiative rate constants are three times higher than the non radiative ones. The strong emissivity of these 4-aminostilbene derivatives can be ascribed to N-aryl-substituted effects which have been previously rationalized by Yang *et al.*⁷¹ Indeed, the N-phenylation on *trans*-4-aminostilbene leads a strong increase of the C=C torsional barrier which reduces the non-radiative rate constant for *trans*-to-*cis* photoisomerization. As a consequence, the strongly fluorescent nature of N-phenyl compounds can be ascribed to a severe reduction of the major non-radiative deactivation channel. In apolar (hexane) and

highly polar (acetonitrile) solvents, the compound **1** remains strongly fluorescent with a radiative deactivation process arising from a single emitting species. In the same media, compounds **2** and **3** are less emissive and their fluorescence lifetime decays are more complex since both compounds clearly exhibit two components (see Fig. S5, †ESI). It should be emphasized that no excitation wavelength dependencies are observed on the fluorescence band shapes. Moreover, the excitation spectra collected at various emission wavelengths match perfectly the absorption spectra of the compounds. It clearly excludes the presence of different conformers at ground states. Therefore, these multicomponent decays presumably denote the presence of local minima within the S_1 surface which stem from a large amplitude relaxation implying electronic and geometrical changes from a fully delocalized Franck-Condon state to a polar excited localized state in one branch of the structures. This assumption is in line with previous calculations^{45, 47} on the excited-states geometry of multibranch D- π -A dipoles which have shown that the excited chromophore undergoes a photoinduced planarization affecting only one branch of the structure and promoting the radiative deactivation from a localized planar intramolecular charge transfer (ICT) state.

TWO-PHOTON ABSORPTION (2PA) PROPERTIES. Two-photon absorption cross-section (δ) measurements have been carried out using two-photon excited fluorescence (2PEF)^{55, 56}. The 2PA spectra have been recorded both in visible (i.e. 480-520 nm) and NIR (i.e. 690-1040nm) ranges using a femtosecond Ti: Sapphire oscillator associated with a second-harmonic generator module. The 2PA spectra of the compounds in THF are presented in Fig. 5 and all related data are summarized in Table 4. In the 690-900 nm range, the 2PA

Table 4. Two-photon absorption parameters of sensitizers **1-3** in visible and NIR regions.

	690-1040 nm range						480-520 nm range	
	Lowest-Energy Peak				Highest-Energy Peak		δ_{MAX}^b (λ_{MAX})	$\delta_{520\text{ nm}}$
	λ_1 / nm	δ_1 / GM	N_{eff}^a	δ_1/N_{eff}^2 / 10^{-2} GM	λ_2 / nm	δ_2 / GM		
1	765	16	16.4	5.9	-	-	139 GM (480 nm)	65
2	795	38	20.4	9.1	720	71	518 GM (500 nm)	252
3	795	67	24.2	11.4	< 690	> 133	651 GM (500 nm)	423

^a Effective number of π -electrons as described by Kuzyk *et al.*⁸³ ^b Maximum 2PA cross-section recorded within the spectral region which does not correspond to a peak maximum.

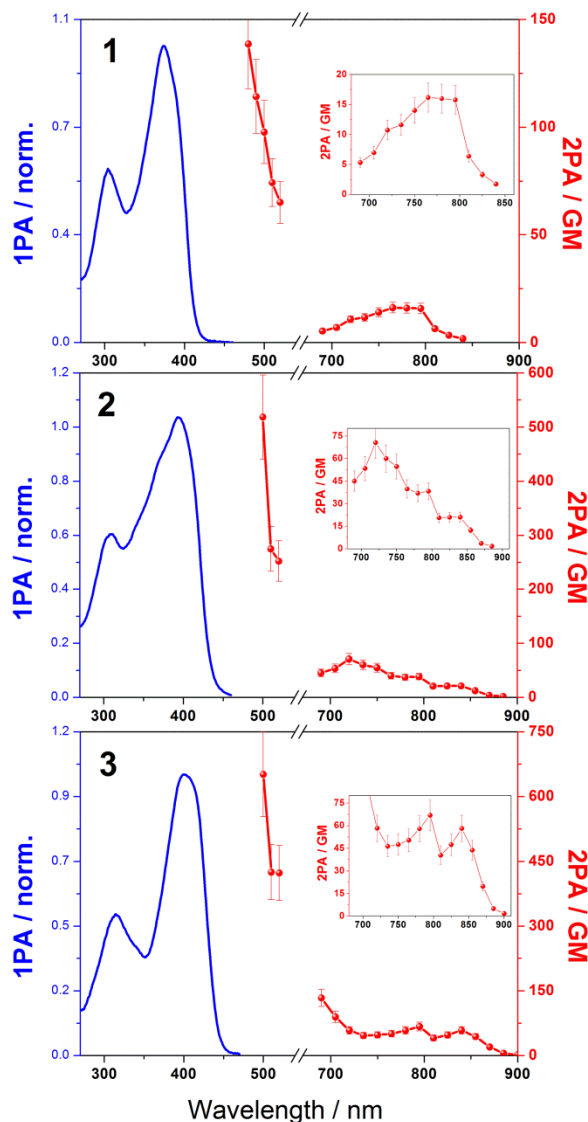


Fig. 5. 1PA (blue lines) and 2PA (red lines) spectra of sensitizers **1-3** in THF. (For sake of clarity the 540-680 nm range was omitted within each 2PA spectrum). Insets: the amplified 2PA in the near-infrared region.

spectrum of **1** consists of a single broad band which matches quite well the 1PA band when plotted against half the excitation wavelength. This effect obviously indicates that the $S_0 \rightarrow S_1$ transition is two-photon allowed as expected for an asymmetric

dipolar molecule. However, **1** exhibits a relatively low δ_{MAX} with a value of ca. 16 GM. According to the simplified two-state model which only includes the ground state S_0 and the lowest excited one S_1 , the δ_{MAX} can be approximated by the following relation^{77, 78}:

$$\delta_{MAX} \approx \frac{2\pi \cdot L^4}{5\epsilon_0^2 n^2 c^2 h} \frac{\Delta\mu_{01}^2 M_{01}^2}{\Gamma} \quad (2)$$

Γ corresponds to the damping factor relative to the two-photon active $S_0 \rightarrow S_1$ transition and it is generally fixed to 0.1 eV which is a typical mean value for conjugated organic derivatives in solution⁷⁹. L is the local field factor ($L = (n^2 + 2)/3$) which corresponds to the enhancement of the optical field in the medium with respect to vacuum. M_{01} is the transition dipole moment relative to the $S_0 \rightarrow S_1$ transition. For compound **1**, M_{01} can be directly calculated from the integrated strength of the longest wavelength 1PA band according to^{80, 81}:

$$M_{01}^2 = \frac{3hc10^3 \ln 10}{8\pi^3 N_A n} \int \epsilon(\nu_a) d(\ln \nu_a) \quad (3)$$

N_A is Avogadro's number and $\epsilon(\nu_a)$ corresponds to the molar extinction coefficient of the 1PA spectrum. The calculation of M_{01} leads to a value of about ca. 7.3 D. Finally, $\Delta\mu_{01}$ corresponds to the permanent dipole moment change between ground state (S_0) and Franck-Condon excited state (S_1^{FC}). This latter parameter can be evaluated according to equation 2 and the experimental value measured for δ_{MAX} (16 GM). As a consequence, the permanent dipole moment change between S_0 and S_1^{FC} is about 3.0 D. This value is 4.7 times lower than that calculated for the relaxed emitting state (see Table 1) and illustrates a weak CT character on the $S_0 \rightarrow S_1$ transition. This is also in line with the very poor solvatochromic behaviour of the longest wavelength band of the 1PA spectrum. The 2PA maximum of **2** which is located around 720 nm ($\delta_1 \sim 70$ GM) is blue shifted with respect to twice the 1PA absorption maximum. According to the dipole selection rules relative to centrosymmetric molecules, the lowest-energy transition is theoretically two-photon forbidden whereas the $S_0 \rightarrow S_2$ one is two-photon allowed. Overall, such rules are almost confirmed since the maximum wavelength of the 2PA band nicely corresponds to the calculated position of the $S_0 \rightarrow S_2$ transition

which was also indicated by our previous anisotropy measurements (see Fig. 3). However, one can observe that the 2PA spectrum of **2** presents a weak shoulder peak around 800 nm ($\delta_1 \sim 40$ GM) which can be assigned to the 2PA forbidden $S_0 \rightarrow S_1$ transition. This breaking in the 2PA selection rules is presumably due to the relaxation of the molecular structure toward a geometry with lower symmetry. Finally, a 2PA band for compound **3** is observed at 795 nm ($\delta \sim 67$ GM) which is in good agreement with twice the 1PA maximum. It is worth noting that δ increases significantly in the high energy side of the NIR spectrum and reaches a value of 133 GM at 690 nm. Such an evolution is commonly observed for three-branched chromophores^{45, 47, 82, 83}. Indeed, the first two degenerate levels (see Scheme 3) are moderately two-photon active with respect to their high-lying third level which is strongly two-photon allowed. As shown in Table 4, the cross-sections of the first 2PA band (δ_1) gradually increase with the number of branches. However, it should be emphasized that δ depends quadratically on the effective number of electrons (N_{eff}) which contribute to the non linear response of the molecule⁸⁴. This parameter can be determined according to the counting method proposed by Kuzyk *et al.*⁸⁵. When normalizing the 2PA cross-section by the square of the effective number of electrons (δ/N_{eff}^2), a direct comparison can be made between the intrinsic 2PA properties within a series of chromophores. This methodology allows, for example, a real quantification of cooperative effects promoted by the multibranching strategy. A clear cooperative trend is observed in our series with an enhancement of the 2PA propensity by a factor 1.54 between the dipole **1** and the V-shaped quadrupole **2** and by a factor 1.93 between the dipole and its octupole **3**.

The measurement of 2PA spectra has been extended to a part of the visible region (i.e. 480-520 nm). In this spectral range, no peak can be clearly distinguished. However, the 2PA cross sections drastically increase when the incident wavelength approaches the lowest energy band of the linear absorption. It must be emphasized that the 1PA is still negligible as confirmed by the quadratic relationship between the fluorescence emission and the incident excitation power (see Fig. S6, †ESI). Interestingly, the corresponding δ_{MAX} are relatively large with respect to those measured in the NIR region (see Table 4). For instance, between the maximum 2PA peak at 795 nm and the maximum value recorded at 500 nm, a 10-fold enhancement of δ is observed for compounds **2** and **3**. This strong increase of the 2PA cross sections should be connected to the 'so-called' one-photon resonance enhancement effect which has been extensively investigated for porphyrin derivatives by Drobizhev *et al.*⁸⁶⁻⁸⁸. According to the classical three-state model which implies the involvement of an intermediate state j within the expression of $\delta(\nu)$, it was demonstrated that the strong 2PA enhancement near the 1PA region stemming from the decrease of the detuning factor ($\nu_j - \nu$) in the denominator of $\delta(\nu)$ when the excitation frequency approaches the one-photon transition frequency.

Hence, all these triphenylamine-based compounds both exhibit high linear absorptivities and relatively large 2PA cross

sections (> 100 GM) in the visible region. When associated with the reducible diphenyliodonium salt a relevant photosensitizing solution can be proposed for the elaboration of an efficient bicomponent one- and two-photon induced acid generator system.

3.2 One- and Two-Photon Sensitizing Strategy.

EXCITED STATES REACTIONS BETWEEN DYES AND IODONIUM SALTS (PAG) IN SOLUTION. Addition of large amount of PAG (\sim mM) in solutions containing sensitizers **1-3** (\sim μ M) does not influence the absorption spectra of the compounds. This excludes any charge-transfer complex formation at ground state. However, the presence of the PAG clearly leads to a fluorescence quenching as illustrated in Fig. S7 (†ESI). In connection with the steady-state fluorescence quenching, the fluorescence lifetime of the compounds gradually decreases with increasing concentration of quenchers. The Stern-Volmer⁸⁹ plots which were obtained from steady-state (Φ_f/Φ_f^0) and time-resolved (τ_f/τ_f^0) measurements both lead to linear correlations as depicted in inset Fig. S7 (†ESI). The Stern-Volmer constants derived from the slopes of the correlations are gathered in Table 5. Values of Φ_f/Φ_f^0 from steady state fluorescence measurements match τ_f/τ_f^0 ratios throughout the Stern-Volmer quenching range. Therefore, we conclude that the quenching of sensitizers mainly proceeds through a dynamic process. Moreover, for all sensitizers, the bimolecular quenching rate constants (k_q) show values ($\sim 2 \times 10^{10} \text{ M}^{-1} \text{ s}^{-1}$) close to the diffusion control limit. According to the strong electron-accepting propensity of Ph_2I^+ , the fluorescence quenching of the dyes in presence of iodonium salts can be ascribed to an efficient photoinduced electron transfer (PeT) process stemming from the excited chromophores to the photoacid generator. If we assume such this PeT proceed from the singlet excited state, the free energy associated to the mechanism can be estimated according to the Rehm-Weller equation:

$$\Delta G_{eT} = E_{ox} - E_{red} - E_{00} + C \quad (4)$$

Where E_{ox} and E_{red} correspond to the oxidation potential of the sensitizers (see Table 1) and the reduction potential the PAG ($E_{red} = -0.2 \text{ V vs. SCE}^{26}$), respectively. E_{00} is the energy of singlet excited state and C is the coulombic energy term characterizing the interaction of the generated radical ion pairs. Since the neutral radical of the iodonium salt is formed during the PeT process, this coulombic term can be neglected. The calculated ΔG_{eT} are listed in Table 5. They clearly exhibit negative values which confirms that PeT process at S_1 state is thermodynamically allowed whatever the compounds. In addition, even though we can not determined the triplet energy (E_T) for our derivatives since they are non phosphorescent even in glassy matrix (e.g. in 2-MTHF at 77 K), the values of E_T should be reasonably within the 1.90–2.13 eV range as previously observed for 4, 4'-disubstitued stilbenes⁹⁰. As a consequence, the photoinduced electron transfer at triplet state

Table 5. Two-photon absorption parameters of sensitizers **1-3** in visible and NIR regions.

	K_{SV}^a / M^{-1}	K_{SV}^b / M^{-1}	k_q^c / $10^9 M^{-1} s^{-1}$	ΔG_{ET} / eV	Φ_H^{+d}	IPA Polym. / 365 nm	2PA Polym. / 532 nm	
						R_p/M_0^e / s^{-1}	τ_{min}^f / ms	$\delta_{\lambda} \cdot \Phi_H^{+g}$ / GM
1	52.9	51.8	25.6	-2.00	0.17	2.7	> 200	11.1
2	62.8	63.2	26.6	-1.89	0.15	3.9	10-20	37.8
3	81.9	80.7	33.3	-1.85	0.18	3.8	10	76.1

^a Stern-Volmer constants derived from steady state measurements. ^b Stern-Volmer constants from lifetime measurements. ^c Quenching rate constants: $k_q = K_{SV}^b/\tau_f$. ^d In N_2 -saturated ACN with $[Ph_2I^+] = 1.5 \times 10^{-3} M$. ^e Irradiance: $45 mW cm^{-2}$. ^f $\langle P \rangle = 0.8 mW$. ^g We approximate $\delta_{532 nm} \approx \delta_{520 nm}$.

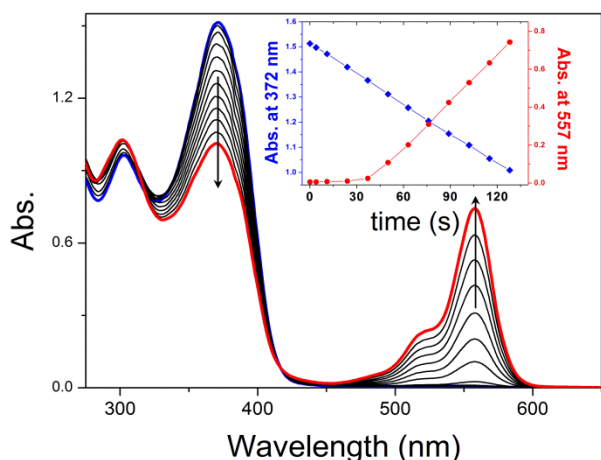
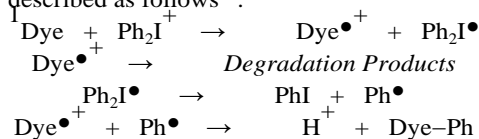


Fig. 6. Evolution of the absorption spectrum of **1** ($4.4 \times 10^{-5} M$ in non-degassed ACN) in presence of Ph_2I^+, PF_6^- ($1.5 \times 10^{-3} M$) during irradiation at 365 nm. Rhodamine B base ($1 \times 10^{-5} M$) is added as acid indicator.

should be also exothermic allowing this process to be considered as an alternative photosensitizing route. However, the PeT from T_1 states is presumably a minor route since excited chromophores mainly deactivate through fluorescence pathway. Fig. 6 shows the changes in the absorption spectrum of a non-degassed solution of **1** in ACN in the presence of a large excess of PAG during photolysis at 365 nm. Note that Rhodamine B base was added as acid indicator. The longest wavelength absorption band of **1** decreases linearly with the irradiation time whereas the band located at 300 nm remains globally invariant. Such changes are also observed for all other derivatives except for **3** which also undergoes a slight band blue shift by about 4 nm. In the primary steps of irradiation, the gradual photobleaching of the compound does not lead to a direct generation of protons as depicted by the induction time of 35 s before the first released protons are detected by the rhodamine B (see inset Fig. 6). Interestingly, this induction time which is of the same order for **2** or **3** can be drastically reduced by a factor 10 when solutions are N_2 -saturated. This point out the inhibiting role of dissolved oxygen in the multistep reactions yielding the proton. Two intermediate species are strongly sensitive to oxygen: excited triplet species and neutral radicals generated after the PeT process. As previously indicated, the role of the former intermediate is negligible. Moreover the rates for dyes photobleaching in the presence of

PAG are much higher than those measured without PAG under air atmosphere. This confirms that the main reactions leading to the dyes photobleaching are related to the photoinduced electron transfer process (i.e. formation of dyes radical cations) and not to a direct reaction between oxygen and excited triplet species. In addition, it should be noted that the stability of the generated triphenylamine-based cations varies markedly with para-substitution⁹¹. They can dimerize or generate multiple by-products^{61, 92, 93}. Therefore one should conclude that the presence of oxygen mainly affects the reactivity of neutral radicals which are generated after PeT process. The photosensitizing mechanism of diphenyliodonium salts can be typically described as follows¹³:



After the PeT process, a triphenylamine-based cation and a neutral diphenyliodonine radical are generated. This latter radical is dissociated into an iodobenzene and a phenyl radical which consecutively combines with the dye cation to finally generate the proton. However, the efficiency of this latter reaction can be drastically reduced since the phenyl radical can be scavenged by O_2 yielding a low reactive peroxy radical. Therefore, the induction time observed before the acid release should correspond to the consumption of the dissolved oxygen which strongly inhibits the last step of the sequential reaction. The photoacid generation quantum yields (Φ_H^+) which were evaluated using the method previously reported by Scaiano *et al.*⁹⁴ are presented in Table 5. All photosensitizing systems exhibit similar efficiencies with an average Φ_H^+ of about ca. 0.17. This value corresponds to 33 % of the acid generation quantum yield measured upon direct excitation of the iodonium salt at 254 nm²⁶. Moreover, it should be noted that our photosensitizing approach has an equivalent efficiency than that obtained when using acridinedione dyes²⁶ but is 6-fold more efficient than strategies employing visible photosensitizers such as benzothiazines⁹⁵ or fluoflavins²⁵.

ONE- AND TWO-PHOTON INDUCED POLYMERIZATION. Fig. 7 shows the FT-RTIR kinetic curves during the monochromatic irradiation (λ_{exc} : 365 nm) of difunctional epoxide formulations containing the iodonium salt (1.5 wt %) associated with our different photosensitizers. Fig. 7A shows the kinetic profiles of formulations with the same mass fraction of photosensitizers

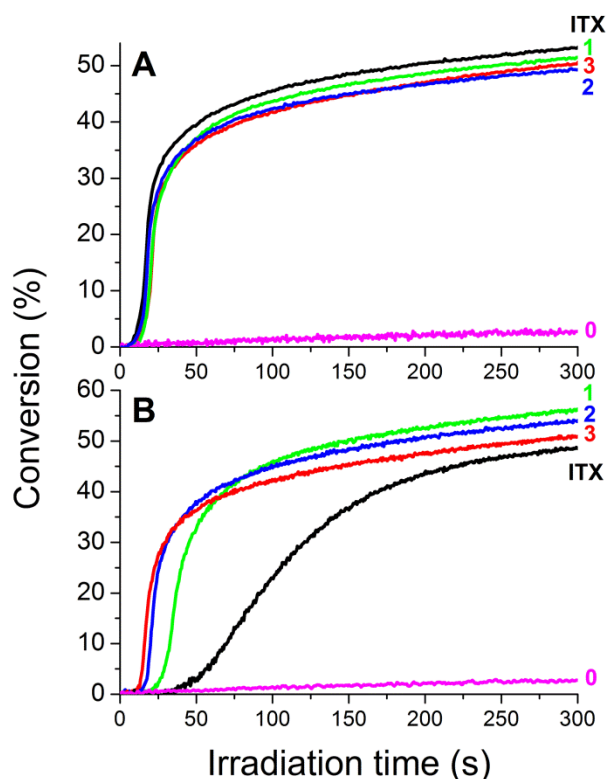


Fig. 7. Conversion vs. time curves for cationic photopolymerization of diepoxide monomer. (λ_{ex} : 365 nm, Irradiance: 45 mW cm⁻²). A. Curve 0: diepoxide resin only with PAG (1.5 wt %). Curves ITX, 1, 2 and 3: Sensitizer (0.15 wt %) + PAG (1.5 wt %). B. Curve 0: diepoxide resin only with PAG (1.5 wt %). Curves ITX, 1, 2 and 3: Isomolar formulations of sensitizer (2.5 mM) + PAG (40 mM \leftrightarrow 1.5 wt %).

(0.15 wt %) whereas Fig. 7B shows the corresponding curves for the same molar concentration (2.5 mM). Moreover, thioxanthone photosensitizer (ITX) was used as a UV-visible reference system^{96, 97}. First, it should be emphasized that the role of photosensitizer is crucial to observe the photopolymerization as indicated by the profile of the formulation 0 which only contains the iodonium salt. The formulations with same mass fraction of photosensitizers are strongly absorbing so that the photoinitiation efficiencies are equivalent for all systems. As a consequence, all kinetic profiles are comparable with: *i*) an induction period of ~ 5 s due to oxygen which inhibits of the neutral radicals ($\text{Ph}\cdot$) generated upon photolysis of the iodonium cation. This induction period can be strongly reduced working with laminated films instead of aerated ones (see Fig. S8, †ESI). *ii*) a maximum polymerization rate (R_p/M_0) of ca. $4.0 \pm 0.1 \text{ s}^{-1}$ *iii*) a final conversion of epoxide functions in the 50-55 % range. Interestingly, working with isomolar formulations enables to have a straightforward correlation between the photosensitizer absorptivity and the amount of generated acid (i.e. $[\text{H}^+] \approx \epsilon_\lambda \cdot \Phi_{\text{H}^+}$). In this condition, it clearly appears from Fig. 7B that the photoinitiation efficiency of the ITX system drops drastically with an induction period of about 40 s and a R_p/M_0 divided by factor 10. With compounds 2 and 3, the amount of initially generated acid seems sufficient to maintain an efficient photopolymerization process as illustrated by the equivalent

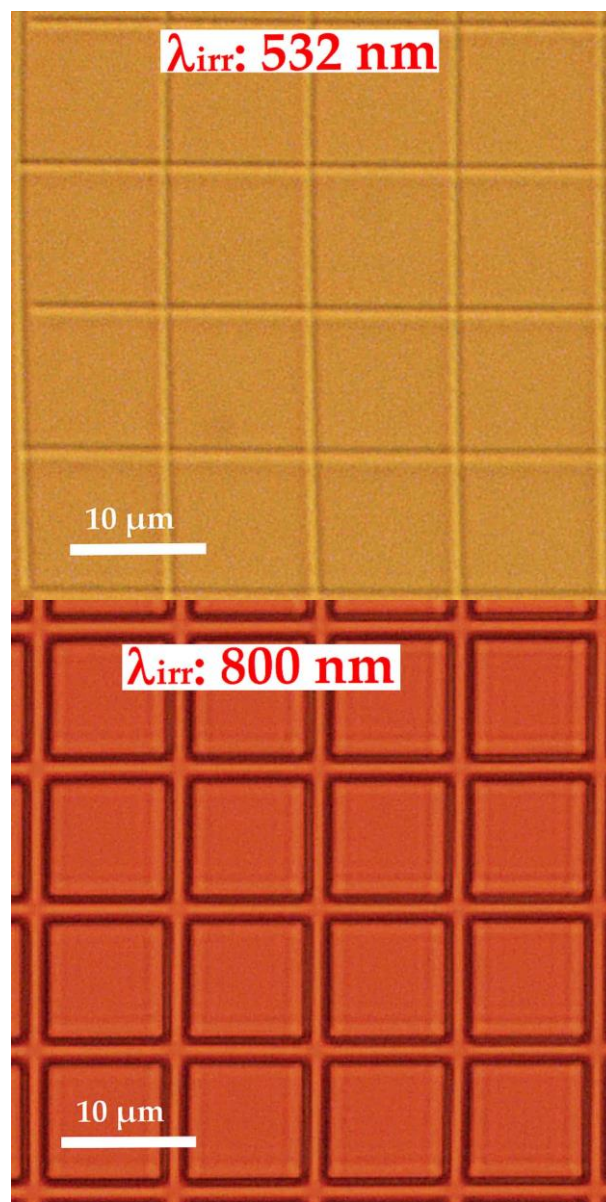


Fig. 8. Microstructures fabricated by two-photon induced polymerization upon excitation at 532 nm ($\langle P \rangle = 0.6 \text{ mW}$, $v = 5 \mu\text{m s}^{-1}$) and at 800 nm ($\langle P \rangle = 15 \text{ mW}$, $v = 5 \mu\text{m s}^{-1}$). Formulation: SU-8 resin with 3 (2.5 mM) and Ph_2I^+ , PF_6^- (40 mM).

values for R_p/M_0 (see Table 5). Finally, the reduced absorptivity of 1 with respect to that of 2 or 3 leads to a 2-fold increase of the induction period with a reduction of R_p/M_0 from 4.0 s^{-1} to 2.7 s^{-1} . Hence, due to their equivalent quantum yields for acid generation, the photoinitiating efficiency of our compounds is clearly dictated by their linear absorptivity. Within this series, such a trend should hold true especially when considering the efficiency of two-photon induced polymerization vs. the two-photon action cross-section (i.e. $[\text{H}^+] \approx \delta_\lambda \cdot \Phi_{\text{H}^+}$). This effect can be illustrated by determining the minimum laser time exposure (τ_{min}) required to write polymerized lines upon two-photon excitation. This simple parameter should be related to the minimum deposited energy necessary to induce two-photon polymerization. In Table 5 are

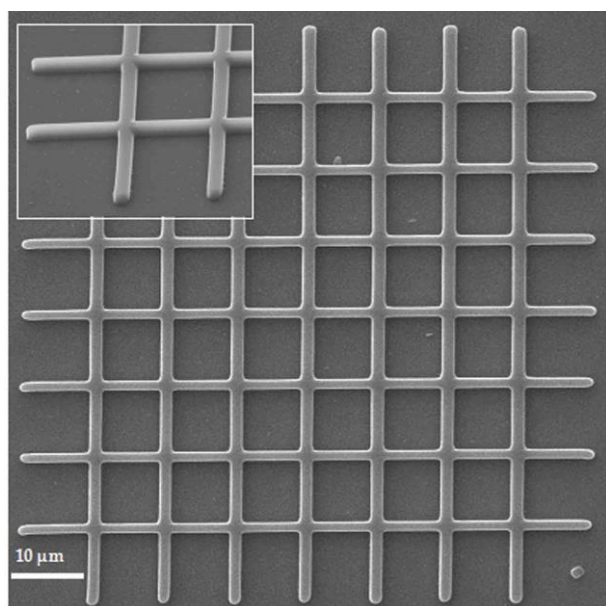


Fig. 9. SEM image of the μ -grid fabricated upon excitation at 800 nm. Inset: Tilted view ($\theta = 45^\circ$)

reported the values of τ_{min} for the isomolar formulations. Each resin was excited at 532 nm using a fixed irradiance at the focal point of 53 GW cm^{-2} . Note that, with the same photonic condition, no photopolymerization is observed at 800 nm which is consistent with a higher reactivity of our bicomponent systems in the visible range. As shown in Table 5, a global tendency can be observed: the decrease of $\delta \cdot \Phi_H^+$ induces the increase of τ_{min} . It is worth noting that both **2** and **3** have superior two-photon initiation efficiency than **1** since their corresponding formulations lead to a minimum time exposure one order of magnitude lower than that measured for **1**. Hence, one clearly confirms that the two-photon *action* cross-section for acid generation constitutes a relevant criterion for the comparison of the two-photon induced polymerization efficiencies at local level.

Finally, to demonstrate the potential applications of these bicomponent systems for multiphoton fabrication at both visible and NIR regions, 2D periodic microstructures were produced using SU-8 resin. This epoxy-based negative photoresist was mixed with the iodonium salt and **3**. Fig. 8 shows the optical transmission microscopy images of two μ -grids written within the SU-8 resin upon excitation at 532 nm and 800 nm respectively. In order to obtain a better feature width of the grids, the exposure parameters were systematically optimized during the fabrication process,⁶⁶ including the excitation power and irradiation time (scan rate). In the end, the polymerizations were performed and optimized upon excitation at 532 nm ($\langle P \rangle = 0.6 \text{ mW}$, $v = 5 \text{ } \mu\text{m s}^{-1}$) and at 800 nm ($\langle P \rangle = 15 \text{ mW}$, $v = 5 \text{ } \mu\text{m s}^{-1}$), respectively. In this conditions, both lasers can produce a regular periodic array. The lines width is of about $0.6 \text{ } \mu\text{m}$ for 532 nm and $1.6 \text{ } \mu\text{m}$ for 800 nm which illustrates the higher writing resolution for short wavelength excitation. Moreover, it should be emphasized that the energy deposited at 532 nm is 7-fold lower than that required for

writing at 800 nm. Fig. 9 also shows the scanning electron microscope (SEM) image of the developed μ -grid which was written at 800 nm. Therefore we clearly demonstrate a synergetic effect upon irradiation at 532 nm in a sense that a better writing resolution is observed concomitant with a higher two-photon initiation.

Conclusions

The linear and nonlinear optical properties of a multibranching compounds have been methodically investigated. The one-photon absorption spectrum of quadrupolar and octupolar systems is dominated by an intensive band which encompasses multiple $S_0 \rightarrow S_n$ transitions whose occurrence is well rationalized on the basis of the Frenkel exciton model. The 2PA spectrum recorded in the NIR region also corroborates the presence of several electronic transitions. A cooperative enhancement of 2PA was observed within this multibranching series with a maximum increase of the intrinsic 2PA cross-section by about 1.9 on going from the dipole to octupole. In the NIR region, the 2PA cross-sections have low-to-moderate values ($\delta \leq 100 \text{ GM}$) but undergo a 10-fold enhancement in the visible range with a δ_{MAX} of about 650 GM for the three-branched derivative. Such triphenylamine-based compounds are very promising candidates for photosensitizing iodonium salts which leads to a mean Φ_H^+ of about 0.17. These reactive bicomponent systems have demonstrated their performances for two-photon lithography in NIR region but also in visible range where a much higher reactivity was observed. By combining advantages of a better writing resolution using short wavelength excitation with a higher efficiency for two-photon initiation, these 2PAGs constitute versatile high-reactive two-photon initiators that can be employed in large spectral range.

Acknowledgements

This work was supported by the National Natural Science Foundation of China (20902069, 51173134, 21074094) and the Open Measuring Fund for Large Instrument and Equipment, Tongji Univ., Fundamental Research Funds for the Central University, Tongji Univ., (0500219159). Supports from the Agence Nationale de la Recherche "Projet Blanc: 2PAGmicrofab (ANR-BLAN-0815-03)" are also gratefully acknowledged. We also thank the meso-centre 'EQUIPEX@MESO' of Strasbourg University for access to HPC resources.

Notes and references

- ^a School of Materials Science and Engineering, Tongji University, 4800 CaoAn Road, 201804, Shanghai, P.R. China.
- ^b Institut de Science des Matériaux de Mulhouse, UMR CNRS 7361, Université de Haute-Alsace, 15 rue Jean Starcky, 68057 Mulhouse, France.
- ^c Institut de Chimie et des Matériaux Paris-Est, UMR 7182, 2-8 rue Henri Dunant, 94320 Thiais. Université Paris-Est Créteil Val de Marne, France.
- ^d Laboratoire de Spectrométrie Physique, UMR CNRS 5588. Université Joseph Fourier, 38402 Saint Martin d'Hères, France.

[†]Laboratoire de Spectrochimie Infrarouge et Raman, UMR CNRS 8516. Université des Sciences et Technologies de Lille. 59655 Villeneuve d'Ascq Cedex, France

[†] Electronic Supplementary Information (ESI) available: [2PEF spectra, Evolution of the absorption spectrum, frontier molecular orbitals, Solvatochromic plots of Stokes shift, Time fluorescence decays, conversion vs. time curves for cationic photopolymerization and so on]. See DOI: 10.1039/b000000x

- S. Sumalekshmy and C. J. Fahrni, *Chem. Mater.*, 2011, **23**, 483-500.
- W. Denk, J. H. Strickler and W. Webb, *Science*, 1990, **248**, 73-76.
- B. H. Cumpston, S. P. Ananthavel, S. Barlow, D. L. Dyer, J. E. Ehrlich, L. L. Erskine, A. A. Heika, S. M. Kuebler, I.-Y. S. Lee, D. McCord-Maughon, J. Qin, H. Röckel, M. Rumi, X.-L. Wu, S. R. Marder and J. W. Perry, *Nature*, 1999, **398**, 51-54.
- W. H. Zhou, S. M. Kuebler, K. L. Braun, T. Y. Yu, J. K. Cammack, C. K. Ober, J. W. Perry and S. R. Marder, *Science*, 2002, **296**, 1106.
- M. Jin, J. P. Malval, D. L. Versace, F. Morlet-Savary, H. Chaumeil, A. Defoin, X. Allonas and J. P. Fouassier, *Chem. Comm.*, 2008, **48**, 6540-6542.
- J.-P. Malval, M. Jin, F. Morlet-Savary, H. Chaumeil, A. Defoin, O. Soppera, T. Scheul, M. Bouriau and P. L. Baldeck, *Chem. Mater.*, 2011, **23**, 3411-3420.
- R. Xia, J.-P. Malval, M. Jin, A. Spangenberg, D. Wan, H. Pu, T. Vergote, F. Morlet-Savary, H. Chaumeil, P. Baldeck, O. Poizat and O. Soppera, *Chem. Mater.*, 2012, **24**, 237-244.
- J.-P. Malval, F. Morlet-Savary, H. Chaumeil, L. Balan, D.-L. Versace, M. Jin and A. Defoin, *J. Phys. Chem. C*, 2009, **113**, 20812-20821.
- H.-B. Sun and S. Kawata, *Two-Photon Photopolymerization and 3D Lithographic Microfabrication*, Berlin, 2004.
- S. Kawata, H.-B. Sun, T. Tanaka and K. Takada, *Nature*, 2001, **412**, 697-698.
- C. N. LaFratta, J. T. Fourkas, T. Baldacchini and R. A. Farrer, *Angew. Chem. Int. ed*, 2007, **46**, 6238-6258.
- G. S. He, L.-S. Tan, Q. Zheng and P. N. Prasad, *Chem. Rev.*, 2008, **108**, 1245-1330.
- M. Shirai and M. Tsunooka, *Prog. Polym. Sci.*, 1996, **21**, 1-45.
- E. Reichmanis, F. M. Houlihan, O. Nalamasu and T. X. Neenan, in *Polymers for Microelectronics*, American Chemical Society, 1993, pp. 2-24.
- E. Reichmanis and F. Thompson Larry, in *Microlithography*, American Chemical Society, 1989, pp. 1-24.
- F. Ortica, C. Coenjarts, J. C. Scaiano, H. Liu, G. Pohlers and J. F. Cameron, *Chem. Mater.*, 2001, **13**, 2297-2304.
- F. Ortica, J. C. Scaiano, G. Pohlers, J. F. Cameron and A. Zampini, *Chem. Mater.*, 2000, **12**, 414-420.
- P. A. Arnold, L. E. Fratesi, E. Bejan, J. Cameron, G. Pohlers, H. Liu and J. C. Scaiano, *Photochem. Photobiol. Sci.*, 2004, **3**, 864-869.
- J.-P. Malval, F. Morlet-Savary, X. Allonas, J.-P. Fouassier, S. Suzuki, S. Takahara and T. Yamaoka, *Chem. Phys. Lett.*, 2007, **443**, 323-327.
- J.-P. Malval, S. Suzuki, F. Morlet-Savary, X. Allonas, J.-P. Fouassier, S. Takahara and T. Yamaoka, *J. Phys. Chem. A*, 2008, **112**, 3879-3885.
- M. Saotome, S. Takano, A. Tokushima, S. Ito, S. Nakashima, Y. Nagasawa, T. Okada and H. Miyasaka, *Photochem. Photobiol. Sci.*, 2005, **4**, 83-88.
- S. Kruger, S. Revuru, C. Higgins, S. Gibbons, D. A. Freedman, W. Yueh, T. R. Younkin and R. L. Brainard, *J. Am. Chem. Soc.*, 2009, **131**, 9862-9863.
- K. J. Schafer, J. M. Hales, M. Balu, K. D. Belfield, E. W. V. Stryland and D. J. Hagan, *J. Photochem. Photobiol. A: Chem.*, 2004, **162**, 497-502.
- J. V. Crivello and J. L. Lee, *Macromolecules*, 1981, **14**, 1141-1147.
- J. Narewska, R. Strzelczyk and R. Podsiadly, *J. Photochem. Photobiol. A: Chem.*, 2010, **212**, 68-74.
- C. Selvaraju, A. Sivakumar and P. Ramamurthy, *J. Photochem. Photobiol. A: Chem.*, 2001, **138**, 213-226.
- J. V. Crivello and J. H. W. Lam, *J. Polym. Sci.: Polym. Chem. Ed.*, 1978, **16**, 2441-2451.
- M. L. Gómez, C. M. Previtali, H. A. Montejano and S. G. Bertolotti, *J. Photochem. Photobiol. A*, 2007, **188**, 83-89.
- S. M. Kuebler, K. L. Braun, W. Zhou, J. K. Cammack, T. Yu, C. K. Ober, S. R. Marder and J. W. Perry, *J. Photochem. Photobiol. A*, 2003, **158**, 163-170.
- T. Yu, C. K. Ober, S. M. Kuebler, W. Zhou, S. R. Marder and J. W. Perry, *Adv. Mater.*, 2003, **15**, 517-521.
- W. Zhou, S. M. Kuebler, K. L. Braun, T. Yu, J. K. Cammack, C. K. Ober, J. W. Perry and S. R. Marder, *Science*, 2002, **296**, 1106-1109.
- W. Zhou, S. M. Kuebler, D. Carrig, J. W. Perry and S. R. Marder, *J. Am. Chem. Soc.*, 2002, **124**, 1897-1901.
- L. Steidl, S. J. Jhaveri, R. Ayothi, J. Sha, J. D. McMullen, S. Y. C. Ng, W. R. Zipfel, R. Zentel and C. K. Ober, *J. Mater. Chem.*, 2009, **19**, 505-513.
- C. Li, L. Luo, S. Wang, W. Huang, Q. Gong, Y. Yang and S. Feng, *Chem. Phys. Lett.*, 2001, **340**, 444-448.
- C. O. Yanez, C. D. Andrade and K. D. Belfield, *Chem. Comm.*, 2009, 827-829.
- M. Jin, H. Xu, H. Hong, J.-P. Malval, Y. Zhang, A. Ren, D. Wan and H. Pu, *Chem. Comm.*, 2013, **49**, 8480-8482.
- Y. Boiko, J. Costa, M. M. Wang and S. Esener, *Optics Express*, 2001, **8**, 571-584.
- K. D. Belfield, K. J. Schafer, Y. Liu, J. Liu, X. Ren and E. W. V. Stryland, *J. Phys. Org. Chem.*, 2000, **13**, 837-849.
- K. D. Belfield and K. J. Schafer, *Chem. Mater.*, 2002, **14**, 3656-3662.
- Y. Murakami, C. A. Coenjarts and C. K. Ober, *J. Photopolym. Sci. Technol.*, 2004, **17**, 115-118.
- W. H. Teh, U. Durig, U. Drechsler, C. G. Smith and H. J. Guentherodt, *J. Appl. Phys.*, 2005, **97**, 054907.
- S. Maruo, K. Ikuta and H. Korogi, *J. Microelectromech. Syst.*, 2003, **12**, 533.
- C. O. Yanez, C. D. Andrade, S. Yao, G. Luchita, M. V. Bondar and K. D. Belfield, *ACS Appl. Mater. Interfaces*, 2009, **1**, 2219-2229.
- H. Yuan, Y. Zhao and F. Wu, *Chem. Mater.*, 2012, **24**, 1371-1377.
- C. Katan, F. Terenziani, O. Mongin, M. H. V. Werts, L. Porrès, T. Pons, J. Mertz, S. Tretiak and M. Blanchard-Desce, *J. Phys. Chem. A*, 2005, **109**, 3024-3037.
- C. Katan, S. Tretiak and J. Even, *Proc. SPIE* 2010, **7712**, 77123D-77123D.

47. C. Katan, S. Tretiak, M. H. V. Werts, A. J. Bain, R. J. Marsh, N. Leonczek, N. Nicolaou, E. Badaeva, O. Mongin and M. Blanchard-Desce, *J. Phys. Chem. B*, 2007, **111**, 9468-9483.
48. F. Terenziani, C. Katan, E. Badaeva, S. Tretiak and M. Blanchard-Desce, *Adv. Mater.*, 2008, **20**, 4641-4678.
49. H. Xia, J. He, B. Xu, S. Wen, Y. Li and W. Tian, *Tetrahedron*, 2008, **64**, 5736-5742.
50. D. Jana and B. K. Ghorai, *Tetrahedron Lett.*, 2012, **53**, 196-199.
51. H. Niu, J. Cai, P. Zhao, C. Wang, X. Bai and W. Wang, *Dyes and Pigments*, 2013, **96**, 158-169.
52. R. Meech and D. Phillips, *J. Photochem.*, 1983, **23**, 193-217.
53. T. J. V. Prazeres, A. Fedorov, S. P. Barbosa, J. M. G. Martinho and M. N. Berberan-Santos, *J. Phys. Chem. A*, 2008, **112**, 5034-5039.
54. D. V. Connor and D. Phillips, *Time correlated single photon counting*, Academic Press, London, 1984.
55. C. Xu and W. W. Webb, *J. Opt. Soc. Am. B*, 1996, **13**, 481-491.
56. M. A. Albota, C. Xu and W. W. Webb, *Appl. Opt.*, 1998, **37**, 7352-7356.
57. C. Martineau, R. An érnian, C. Andraud, I. Wang, M. Bouriau and P. L. Baldeck, *Chem. Phys. Lett.*, 2002, **362**, 291-295.
58. K. D. Belfield, M. V. Bondar, F. E. Hernandez, O. V. Przhonska and S. Yao, *J. Phys. Chem. B*, 2007, **111**, 12723-12729.
59. M. Montalti, A. Credi, L. Prodi and M. T. Gandolfi, *Handbook of Photochemistry, Third Ed.*, CRC Press, Boca Raton, 2006.
60. J.-P. Malval, C. Chaimbault, B. Fischer, J.-P. Morand and R. Lapouyade, *Res. Chem. Interim.*, 2001, **27**, 21-34.
61. J. P. Malval, J. P. Morand, R. Lapouyade, W. Rettig, G. Jonusauskas, J. Oberle, C. Trieflinger and J. Daub, *Photochem. Photobiol. Sci.*, 2004, **3**, 939-948.
62. J. Guillon, P. Sonnet, J.-P. Malval, S. Massip, I. Gosse, J.-M. L éger, R. Lapouyade, J. Rochette, J.-P. Monti and C. Jarry, *Supramol. Chem.*, 2002, **14**, 437-451.
63. P. Hapiot, L. D. Kispert, V. V. Kononov and J.-M. Sav éant, *J. Am. Chem. Soc.*, 2001, **123**, 6669-6677.
64. J. V. Crivello and R. Narayan, *Macromolecules*, 1996, **29**, 439-445.
65. J. V. Crivello and R. Narayan, *Macromolecules*, 1996, **29**, 433-438.
66. M. Stoneman, M. Fox, C. Zeng and V. Raicu, *Lab on a Chip*, 2009, **9**, 819-827.
67. S. C. Laza, M. Polo, A. A. R. Neves, R. Cingolani, A. Camposeo and D. Pisignano, *Advanced Materials*, 2012, **24**, 1304-1308.
68. S. Aloise, Z. Pawlowska, C. Ruckebusch, M. Sliwa, J. Dubois, O. Poizat, G. Buntinx, A. Perrier, F. Maurel, P. Jacques, J.-P. Malval, L. Poisson, G. Piani and J. Abe, *Phys. Chem. Chem. Phys.*, 2012, **14**, 1945-1956.
69. M. J. Frisch, in *Gaussian 09, Revision B.01, Gaussian, Inc., Wallingford CT*, Wallingford CT, 2009.
70. R. P. Subrayan, J. W. Kampf and P. G. Rasmussen, *J. Org. Chem.*, 1994, **59**, 4341-4345.
71. J.-S. Yang, S.-Y. Chiou and K.-L. Liao, *J. Am. Chem. Soc.*, 2002, **124**, 2518-2527.
72. D. Beljonne, W. Wenseleers, E. Zojer, Z. Shuai, H. Vogel, S. J. K. Pond, J. W. Perry, S. R. Marder and J. L. Br ádas, *Adv. Funct. Mater.*, 2002, **12**, 631.
73. A. S. Davydov, *Theory of molecular excitons*, Plenum Press, New York, 1971.
74. G. Alcaraz, L. Euzenat, O. Mongin, C. Katan, I. Ledoux, J. Zyss, M. Blanchard-Desce and M. Vaultier, *Chem. Comm.*, 2003, **0**, 2766-2767.
75. E. Lippert, *Z. Naturforsch.*, 1955, **10a**, 541-545.
76. N. Mataga, Y. Kaifu and M. Koizumi, *Bull. Chem. Soc. Jpn.*, 1955, **28**, 690-691.
77. T. Kogej, D. Beljonne, F. Meyers, J. W. Perry, S. R. Marder and J. L. Br ádas, *Chem. Phys. Lett.*, 1998, **298**, 1-6.
78. M. Barzoukas and M. Blanchard-Desce, *J. Chem. Phys.*, 2000, **113**, 3951-3959.
79. M. Rumi, J. E. Ehrlich, A. Heikal, J. W. Perry, S. Barlow, Z. Y. Hu, D. McCord-Maughon, T. C. Parker, H. Rockel, S. Thayumanavan, S. R. Marder, D. Beljonne and J. L. Br ádas, *J. Am. Chem. Soc.*, 2000, **122**, 9500-9510.
80. I. B. Berlman, *J. Chem. Phys.*, 1970, **52**, 5616.
81. I. B. Berlman and O. J. Steingraber, *J. Chem. Phys.*, 1965, **43**, 2140.
82. Y.-Z. Cui, Q. Fang, G. Xue, G.-B. Xu, L. Yin and W.-T. Yu, *Chem. Phys.*, 2005, **34**, 644-645.
83. B. R. Cho, K. H. Son, S. H. Lee, Y.-S. Song, Y.-K. Lee, S.-J. Jeon, J. H. Choi, H. Lee and M. Cho, *J. Am. Chem. Soc.*, 2001, **123**, 10039-10045.
84. J. P. Moreno and M. G. Kuzyk, *J. Chem. Phys.*, 2005, **123**, 194101-194113.
85. M. G. Kuzyk, *J. Chem. Phys.*, 2003, **119**, 8327-8334.
86. M. Drobizhev, A. Karotki, M. Kruk, M. Z. Mamardashvili and A. Rebane, *Chem. Phys. Lett.*, 2002, **361**, 504-512.
87. M. Drobizhev, A. Karotki, M. Kruk and A. Rebane, *Chem. Phys. Lett.*, 2002, **355**, 175-182.
88. M. Drobizhev, Y. Stepanenko, Y. Dzenis, A. Karotki, A. Rebane, P. N. Taylor and H. L. Anderson, *J. Am. Chem. Soc.*, 2004, **126**, 15352-15353.
89. J. R. Lakowicz, *Principles of Fluorescence Spectroscopy*, Springer Science, New York, 2006.
90. H. Gä rner, *J. Phys. Chem.*, 1989, **93**, 1826-1832.
91. N. Cocherel, P. Leriche, E. Ripaud, N. Gallego-Planas, P. Frere and J. Roncali, *New J. Chem.*, 2009, **33**, 801-806.
92. E. T. Seo, R. F. Nelson, J. M. Fritsch, L. S. Marcoux, D. W. Leedy and R. N. Adams, *J. Am. Chem. Soc.*, 1966, **88**, 3498.
93. K. Yuan Chiu, T. Xiang Su, J. Hong Li, T.-H. Lin, G.-S. Liou and S.-H. Cheng, *J. Electroan. Chem.*, 2005, **575**, 95-101.
94. G. Pohlner, J. C. Scaiano and R. Sinta, *Chem. Mater.*, 1997, **9**, 3222-3230.
95. R. Podsiadly, *J. Photochem. Photobiol A: Chem.*, 2009, **208**, 147-153.
96. G. Manivannan and J. P. Fouassier, *J. Polym. Sci. Part A: Polym. Chem.*, 1991, **29**, 1113.
97. J.-D. Cho and J.-W. Hong, *Eur. Polym. J.*, 2005, **41**, 367-374.